



HAL
open science

Implementation of the boundary integral method on MIMD systems for electromagnetic scattering problems

Thierry Jacques, Laurent Nicolas, Christian Vollaire

► **To cite this version:**

Thierry Jacques, Laurent Nicolas, Christian Vollaire. Implementation of the boundary integral method on MIMD systems for electromagnetic scattering problems. *IEEE Transactions on Magnetics*, 2000, 36 (4 Part 1), pp.1479-1483. hal-00141509

HAL Id: hal-00141509

<https://hal.science/hal-00141509>

Submitted on 18 Apr 2007

HAL is a multi-disciplinary open access archive for the deposit and dissemination of scientific research documents, whether they are published or not. The documents may come from teaching and research institutions in France or abroad, or from public or private research centers.

L'archive ouverte pluridisciplinaire **HAL**, est destinée au dépôt et à la diffusion de documents scientifiques de niveau recherche, publiés ou non, émanant des établissements d'enseignement et de recherche français ou étrangers, des laboratoires publics ou privés.

Implementation of the Boundary Integral Method on MIMD Systems for Electromagnetic Scattering Problems

Thierry Jacques, Laurent Nicolas, and Christian Vollaire

Abstract—The boundary integral method is used to solve problems of scattering by perfect electric conducting or perfect dielectric bodies. Because this method requires large memory storage, it is implemented on a distributed memory parallel computer. The assembling is performed by nodal contribution, and the BiCGStab(m) algorithm is used for solving. Performances are analyzed using several large problems.

Index Terms—Distributed memory systems, integral equations, numerical analysis, parallel algorithms.

I. INTRODUCTION

IN [1], SEVERAL examples of parallelization of the different numerical methods used in computational electromagnetics are described. It is also shown that only a few attempts to parallelize the boundary element method (BEM) have been made. This method shows however several advantages: first, only the material interfaces have to be discretized. Second, it takes implicitly into account the decrease of the field at infinity. On the other hand, it is applicable to nonlinear materials with difficulty. Moreover, it generates a full non-Hermitian matrix which requires large memory capabilities. This last point explains why only parallel computers are able to offer the required power to handle large devices.

The objective of this paper is to show how the BEM has been implemented on a distributed memory parallel computer, a Cray T3E. The frequency-domain formulations for electromagnetic scattering by both perfect electric conducting (PEC) or perfect dielectric bodies are first described. The parallel implementation is then presented. Special attention is paid to the reduction of the storage of the matrix and to the communication between the processors. Parallel efficiency is finally analyzed using several examples.

II. BEM FORMULATIONS FOR ELECTROMAGNETIC SCATTERING

As shown in Fig. 1, an incident wave (frequency f , beat ω) is perturbed by an object of boundary Σ .

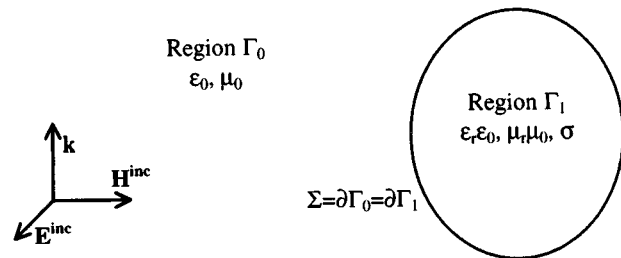


Fig. 1. Description of the problem. The electromagnetic properties of the material are the conductivity (σ), the permittivity ($\epsilon_r \epsilon_0$) and the permeability ($\mu_r \mu_0$).

A. Scattering by a PEC Body

By writing the Magnetic Field Integral Equation at a point x on the surface Σ of the scatterer, we get [2]:

$$\begin{aligned} \mathbf{J}(x) &= 2\mathbf{n} \times \mathbf{H}^{\text{inc}}(x) + \frac{\mathbf{n}}{2\pi} \times \iint_{\Sigma} (\mathbf{J} \times \nabla G_0) ds \\ E_n &= 2\mathbf{E}^{\text{inc}}(x) \cdot \mathbf{n} + \frac{\mathbf{n}}{2\pi} \cdot \iint_{\Sigma} (j\omega\mu_0 \mathbf{J} G_0 + E_n \nabla G_0) ds \end{aligned} \quad (1)$$

where

- \mathbf{J} is the electric current density,
- E_n is normal electric field,
- G_0 is Green's function,
- \mathbf{n} is the unit normal vector to the surface Σ and
- $\mathbf{H}^{\text{inc}}, \mathbf{E}^{\text{inc}}$ are the magnetic and electric incident fields.

Only the first equation of this formulation is required to solve the scattering problem. It leads to 3 complex degrees of freedom per node.

B. Scattering by a Dielectric Body

The properties of the material are its permittivity $\epsilon_r \epsilon_0$ and its permeability $\mu_r \mu_0$. For each term, two equations are obtained by applying the Green's theorem in the inner and outer regions. By taking into account the boundary conditions at material interfaces, these two equations are coupled in order to avoid numerical problems due to the gradient term ($\nabla G_0 - \nabla G_1$). G_0 and G_1 are Green's function of respective wave number $k_0 = \omega\sqrt{\epsilon_0\mu_0}$ and $k_1 = k_0\sqrt{\epsilon_r\mu_r}$, and $\alpha = j\sqrt{\epsilon_0/\mu_0}$. By denoting the normal magnetic and electric fields H_n and E_n , the electric and

Manuscript received October 25, 1999.

The authors are with the CEGELY, UPRESA CNRS 5005, Ecole Centrale de Lyon, BP 163, 69131 Ecully cedex, France (e-mail: {tjacques; laurent; vollaire}@eea.ec-lyon.fr).

Publisher Item Identifier S 0018-9464(00)06618-8.

magnetic current densities \mathbf{J} and \mathbf{K} , the following equations may be obtained:

$$\begin{aligned}
\frac{1+\mu_r}{2}\mathbf{J} &= \mathbf{n} \times \mathbf{H}^{\text{inc}} + \frac{\mathbf{n}}{4\pi} \times \iint_{\Sigma} [k_0 \mathbf{K} (G_0 - \varepsilon_r \mu_r G_1) \\
&\quad + \mu_r H_n (\nabla G_0 - \nabla G_1) \\
&\quad + \mathbf{J} \times (\nabla G_0 - \mu_r \nabla G_1)] ds \\
\frac{1+\mu_r}{2}H_n &= \mathbf{n} \cdot \mathbf{H}^{\text{inc}} + \frac{\mathbf{n}}{4\pi} \cdot \iint_{\Sigma} [k_0 \mathbf{K} (G_0 - \varepsilon_r G_1) \\
&\quad + H_n (\mu_r \nabla G_0 - \nabla G_1) \\
&\quad + \mathbf{J} \times (\nabla G_0 - \nabla G_1)] ds \\
\frac{1+\varepsilon_r}{2}\mathbf{K} &= \alpha \mathbf{n} \times \mathbf{E}^{\text{inc}} + \frac{\mathbf{n}}{4\pi} \times \iint_{\Sigma} [k_0 \mathbf{J} (G_0 - \varepsilon_r \mu_r G_1) \\
&\quad + \varepsilon_r E_n (\nabla G_0 - \nabla G_1) \\
&\quad + \mathbf{K} \times (\nabla G_0 - \varepsilon_r \nabla G_1)] ds \\
\frac{1+\varepsilon_r}{2}E_n &= \alpha \mathbf{n} \cdot \mathbf{E}^{\text{inc}} + \frac{\mathbf{n}}{4\pi} \cdot \iint_{\Sigma} [k_0 \mathbf{J} (G_0 - \mu_r G_1) \\
&\quad + E_n (\varepsilon_r \nabla G_0 - \nabla G_1) \\
&\quad + \mathbf{K} \times (\nabla G_0 - \nabla G_1)] ds
\end{aligned} \tag{2}$$

This formulation may be seen as the frequency-domain version of the time-domain formulation found in [3]. The number α has been chosen so that the variables and the coefficients of the matrix have the same size, leading to a better conditioning of the matrix. Eight complex degrees of freedom are required at each mesh node.

C. Numerical Solving

The numerical discretization is performed by using second order surface finite elements (triangular or quadrilateral elements). Ten nodes per wavelength ($\lambda = 2\pi/k_0$ for a PEC body, $\lambda = 2\pi/k_1$ for a dielectric body) are required for a good accuracy. Regular surface integrals are computed using Gauss integration. Singular integral equations are computed analytically [4].

On a geometrical discontinuity such as edges or corners, the electromagnetic fields are discontinuous, leading to indefinite integrals. Half-discontinuous finite elements are then used in

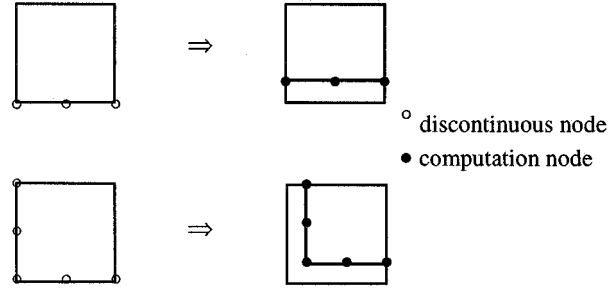


Fig. 2. Half-discontinuous surface finite elements.

order to avoid this difficulty[5]: depending on the type of discontinuity, the points on the edges are separated in two or three computation nodes and moved toward the interior of the elements (Fig. 2).

D. Validation

Validation has been first performed using the analytical solution of the scattering by a perfect electric conducting sphere [6]. As shown in Fig. 3, the maximal relative error between computed and analytical solutions is about 0.25% for 384 quadrilateral finite elements.

The half-discontinuous elements have been validated by comparison with the results provided by the finite element method [9]. Same method has been used for the case of scattering by a dielectric body.

III. PARALLEL IMPLEMENTATION

A. Reduction of the Storage

These formulations generate a full non-Hermitian matrix. For a n -nodes mesh, the storage of the matrix requires $18n^2$ real data for a PEC body and $128n^2$ real data for a dielectric body. For a PEC body, each node generates three rows of the global matrix, corresponding to the three components of the field. The global matrix has the following form of (3) as shown at the bottom of the page, where (n_x, n_y, n_z) is the vector normal to the surface at node. The submatrices located on the diagonal of the global

$$\begin{aligned}
A &= \begin{pmatrix} d_1 I_3 & b_{1,2} & \cdots & b_{1,n} \\ b_{2,1} & \ddots & & \vdots \\ \vdots & & \ddots & b_{n-1,n} \\ b_{n,1} & \cdots & b_{n,n-1} & d_n I_3 \end{pmatrix} \\
b_{ij} &= \begin{pmatrix} c_{ijz}n_{iz} + c_{ijy}n_{iy} & -c_{ijx}n_{iy} & -c_{ijx}n_{iz} \\ -c_{ijy}n_{ix} & c_{ijx}n_{ix} + c_{ijz}n_{iz} & -c_{ijy}n_{iz} \\ -c_{ijz}n_{ix} & -c_{ijz}n_{iy} & c_{ijx}n_{ix} + c_{ijy}n_{iy} \end{pmatrix} \\
c_{iju} &= - \sum_{x_j \in K} \iint_K N_{jK} (1 + jkr) e^{-jkr} \frac{u_i - u_K}{r^3} ds \quad \text{with } u = x, y, z \\
d_i &= 2\pi + c_{ii}n_i
\end{aligned} \tag{3}$$

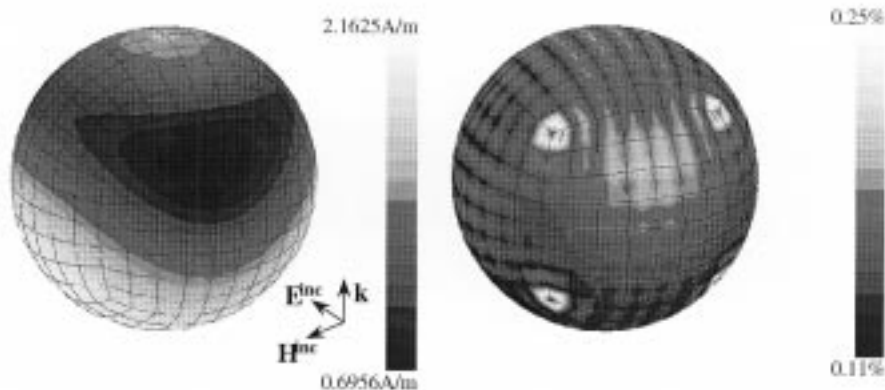


Fig. 3. Scattering of a 600 MHz plane wave by a perfect electric conductor sphere. Visualization of the magnitude of the electric current density (left, in A/m) and the relative error (right, in %).

TABLE I
COMPUTATION TIMES (IN S)/NUMBER OF ITERATIONS OF BICGSTAB(4) FOR THE PEC AND OF BICGSTAB(2) FOR THE DIELECTRIC CYLINDER

PEC cylinder			
Degrees of freedom	4662	6966	9846
12 processors	553 s./ 11 it.	1224 s./ 28 it..	2735 s./ 26 it.
32 processors	569 s./ 11 it.	1266 s./ 28 it.	2912 s./ 28 it.
64 processors	607 s./ 11 it.	1349 s./ 30 it.	3122 s./ 30 it.
Dielectric cylinder			
Degrees of freedom	12432	18576	26256
12 processors	1083 s./ 4 it.	2344 s./ 4 it..	4784 s./ 5 it.
32 processors	1095 s./ 4 it.	2397 s./ 4 it.	4862 s./ 5 it.
64 processors	1127 s./ 4 it.	2451 s./ 4 it.	4956 s./ 5 it.

matrix are proportional to the identity matrix. For each node, only the coefficients $(c_{ijx}, c_{ijy}, c_{ijz})$ are stored, such as the diagonal coefficient and the normal vector. The global storage may consequently be reduced to $6n^2$ real data.

The storage may be reduced in the same manner to $16n^2$ real data for the dielectric body. With a direct method to solve the matrix system, this reduction would be useless since this method requires memory to achieve calculations. However, even when using this trick, parallel computing remains unavoidable to compute large scale devices.

B. Parallel Implementation

The entire data file is duplicated on each processor. The matrix is row-distributed on the processors, and the global system matrix is assembled per node. Hence no communication between the processors is required during this stage, and the speedup is optimal.

The matrix system is solved with the BiCGStab(*m*) algorithm [7]. A complex left diagonal preconditioning is used in the case of a perfect electric conductor, while a complex left block diagonal preconditioning is used in the case of a dielectric body. A diagonal preconditioning has been preferred since the submatrix on the diagonal is dominant. A right preconditioning would require that each processor knows the whole preconditioning matrix and calculates the whole preconditioned vector before the matrix-vector multiplication. On the other hand, a left preconditioning needs less memory and less computation since it is local.

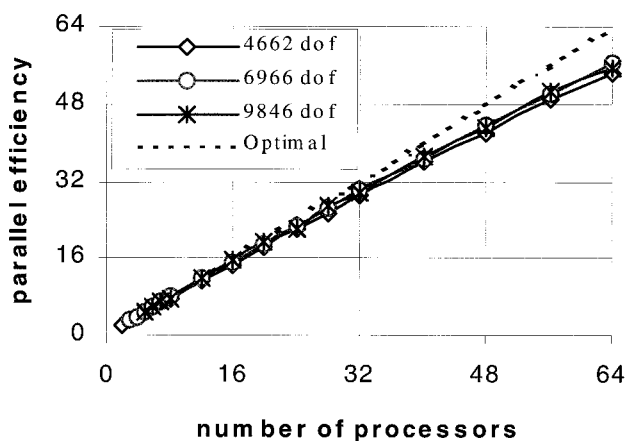


Fig. 4. Parallel efficiency for several number of degrees of freedom. Scattering of a 3 GHz plane wave by a PEC cylinder.

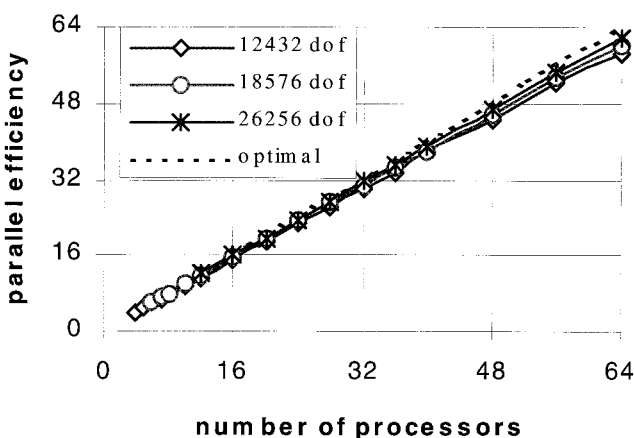


Fig. 5. Parallel efficiency for several number of degrees of freedom. Scattering of a 900 MHz plane wave by a dielectric cylinder.

At each iteration, $2m$ matrix-vector multiplications are required. The BiCGStab(*m*) algorithm is parallelized in order to minimize the communications between the processors: only $2m$ message passing are required per iteration. Each processor computes only a part of the matrix-vector multiplication and some

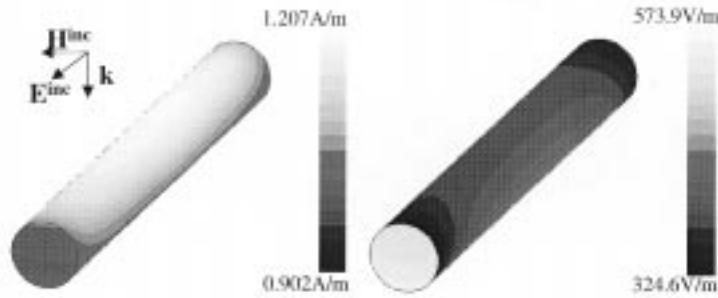


Fig. 6. Scattering of a 900 MHz plane wave by a dielectric cylinder. Visualization of magnetic (left, in A/m) and electric fields (right, in V/m) on the surface of the cylinder.

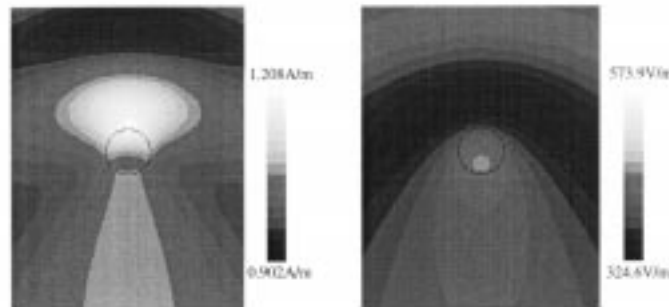


Fig. 7. Scattering of a 900 MHz plane wave by a dielectric cylinder. Visualization of magnetic (left, in A/m) and electric (right, in V/m) fields in the cross-section located in the middle of the cylinder.

partial inner products. On the other hand, it performs all total vector sums and it calculates all correlation coefficients.

The exchange of partial data between processors is achieved by using PVM library. There are two ways to pass messages:

- 1) Broadcast: each processor sends the partial inner product vector to the other processors. With p processors and a total vector of length N , this method requires $p(p-1)$ messages of size N/p , leading to a total exchange of $N(p-1)$ data.
- 2) Master-slave mode: each processor sends the partial result to the first processor which adds first partial inner products and vectors and then returns the whole result. This method requires the exchange of $(p-1)$ messages of size N/p and $(p-1)$ messages of size N , leading to a total exchange of $N(p - (1/p))$ data.

The message passing may generate negligible errors due to the 32 bits implementation of PVM while computations are performed in 64 bits. The broadcast method broadcasts these errors: after a few thousands of message passing, a residual vector may be slightly different from a processor to another, leading to compromise the convergence of the algorithm.

Consequently, the master-slave mode has been chosen as parallel strategy. A synchronization between processors is then carried out before and after each message passing.

C. Algorithm

The solving is performed using the BiCGStab(m) algorithm, since it appears very attractive for non symmetric matrix [8]. An

iteration may be seen as a step of the biconjugate gradient algorithm followed by a step of the GMRES(m) algorithm: it tries to minimize the residual vector according to $m+1$ particular directions. The BiCGStab(m) algorithm is less parallelized than the BiCGStab algorithm because all inner products are not parallelized. On the other hand, it is more robust and converges more quickly for large problems with half-discontinuous elements. The smaller the number of nodes per wavelength is, the larger has to be the number m , in order to allow the convergence of the iterative method: the diagonal term becomes smaller while the contributions of the adjacent nodes become greater. The parameter m is actually chosen according to our experience: it depends on the frequency, on the size of the mesh and on the number of processors.

Regarding the parallel implementation of the BiCGStab algorithm, each processor computes only a part of the solution because the algorithm uses the residual vector to perform the calculations.

IV. PARALLEL PERFORMANCES

The first test problem is the scattering of a 3 GHz plane wave by a PEC cylinder. Its length goes from 2.5λ to 6λ , and its radius is equal to 0.5λ . The second example is the scattering of a 900 MHz plane wave by a dielectric cylinder ($\mu_r = 1$, $\epsilon_r = 2$) of same dimensions. Computations are performed on a Cray T3E (Table I). Results are presented in terms of parallel efficiency, since some problems cannot be computed on one processor: if the minimal number of processors which can be used

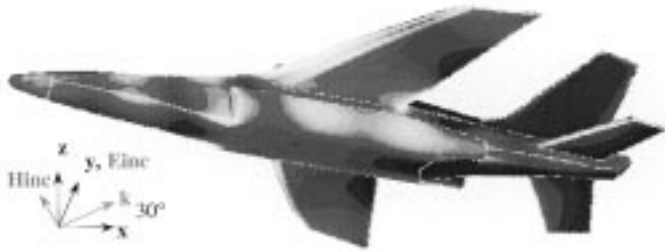


Fig. 8. Scattering of a 100 MHz plane wave by a plane considered as a perfect electric conductor. Visualization of magnetic field (in A/m).

is n , the reference computation time obtained on these n processors leads to a parallel efficiency equal to n .

The parallel efficiency remains high when the number of processors increases (Figs. 4 and 5). Two reasons can be underlined. First, the assembling stage remains dominating (From 70–85% of the total time), with a speedup nearly optimal. Second, the main stage of the solver is the matrix-vector multiplication, which is parallelized. Furthermore, the computing load is well distributed over the processors because each processor performs the same number of operations.

V. NUMERICAL EXAMPLES

The first numerical example is the scattering of a 900 MHz plane wave by a dielectric cylinder ($\mu_r = 1$, $\varepsilon_r = 2$). Its length and its diameter are respectively equal to 1.2λ and 0.075λ . Fig. 7 shows the magnetic and electric fields computed on the surface of the cylinder. It is meshed with 2322 nodes. The calculation has required 2400 seconds with 32 processors on a Cray T3E. Fig. 7 shows the fields computed in a cross section.

The computation of the scattering of a 100 MHz plane wave by an airplane is presented as large example. The solving has been carried out with 64 processors of a Cray T3E. The length of the plane is equal to 11.7 meters. The mesh is made of 2928 finite elements and 10 291 nodes. The calculation required 20

iterations of BiCGStab(12) and has been performed in 35 425 seconds (total time) on a Cray T3E.

VI. CONCLUSION

The parallel implementation of the boundary element method for electromagnetic scattering analysis is presented. The mesh is distributed equally over each processors and the assembling of the full matrix is performed by nodes. This stage is carried out without message passing between the processors. The solving is performed using the BiCGStab(m) algorithm. The parallel efficiency of this solver is excellent, since the parallelized matrix-vector multiplication constitutes its main stage. As shown by the example of scattering by a PEC airplane, the computation of large problems using the BEM is then made possible.

REFERENCES

- [1] L. Nicolas and C. Vollaire, "A survey of computational electromagnetics on MIMD systems," in *International Conference on Parallel Computing in Electrical Engineering*, Bialystok, September 2–5, 1998, pp. 7–19.
- [2] A. J. Poggio and E. K. Miller, "Integral equation methods of three-dimensional scattering problems," in *Computer Techniques for Electromagnetics*, R. Mittra, Ed. Oxford: Pergamon, 1973, pp. 159–265.
- [3] E. Schlemmer, W. M. Rucker, and K. R. Richter, "Calcul des champs électromagnétiques diffractés par un obstacle diélectrique tridimensionnel par éléments de frontière en régime transitoire," *IEEE Journal Physique III*, pp. 2115–2126, November 1992.
- [4] C. J. Huber, W. Rieger, M. Haas, and W. M. Rucker, "The numerical treatment of singular integrals in boundary element calculations," in *7th International IGTE Symposium*, 1996, pp. 368–373.
- [5] S. Rêgo and J. J. Do, "Acoustic and elastic wave scattering using boundary elements," in *Computational Mechanics Publications*, UK, 1994.
- [6] R. F. Harrington, *Field Computation by Moment Methods*. New York: MacMillan, 1968.
- [7] G. L. G. Sleijpen and D. R. Fokkema, "BiCGStab(1) for linear equations involving unsymmetric matrices with complex spectrum," *ETNA*, vol. 1, pp. 11–32, September 1993.
- [8] H. A. Van der Vorst, "BiCGStab a fast and smoothly converging variant of BiCG for the solution of nonsymmetric linear systems," *SIAM J. Science Statist. Comput.*, vol. 13, pp. 631–644, 1992.
- [9] C. Vollaire, L. Nicolas, and A. Nicolas, "Finite elements coupled with absorbing boundary conditions on parallel distributed memory computer," *IEEE Transactions on Magnetics*, vol. 33, no. 2, pp. 1448–1451, March 1997.